View metadata, citation and similar papers at core.ac.uk
brought to you by CORE
provided by Hochschulschriftenserver - Universität Frankfurt am Main

arXiv:nucl-th/9903041 v2 26 Aug 1999

Relativistic Hartree approach including both positive- and negative-energy bound states

G. Mao, H. Stöcker, W. Greiner

Institut für Theoretische Physik der J. W. Goethe-Universität

Postfach 11 19 32, D-60054 Frankfurt am Main, Germany

(December 1, 2005)

We develop a relativistic model to describe the bound states of positive energy and negative energy in finite nuclei at the same time. Instead of searching for the negative-energy solution of the nucleon's Dirac equation, we solve the Dirac equations for the nucleon and the anti-nucleon simultaneously. The single-particle energies of negative-energy nucleons are obtained through changing the sign of the single-particle energies of positive-energy anti-nucleons. The contributions of the Dirac sea to the source terms of the meson fields are evaluated by means of the derivative expansion up to the leading derivative order for the one-meson loop and one-nucleon loop. After refitting the parameters of the model to the properties of spherical nuclei, the results of positive-energy sector are similar to that calculated within the commonly used relativistic mean field theory under the no-sea approximation. However, the bound levels of negative-energy nucleons vary drastically when the vacuum contributions are taken into account. It implies that the negative-energy spectra deserve a sensitive probe to the effective interactions in addition to the positive-energy spectra.

PACS number(s): 21.60.-n; 21.10.-k

I. INTRODUCTION

The extension of the periodic system has a long history in chemistry and physics. Particularly at the end of the sixties and the beginning of the seventies, the time when heavy-ion collisions had its advent, the idea of super-heavy elements emerged. Besides the extension of the periodic system to the *islands of super-heavy nuclei* within the proton Z- and neutron N-axis, there exist two fascinating direction, i.e., to extend Z and N into the negative sector, $\bar{Z}$ and $\bar{N}$, and into the multistrangeness dimension. The first idea was put forward in detail in Ref. [1] where a *collective anti-matter production mechanism* was proposed. The main physical considerations are the following: In the relativistic treatment of nuclear phenomena, one uses the Dirac equation to describe nucleons in nuclei

$$[\boldsymbol{\alpha} \cdot \mathbf{p} + \beta(M_N + S) + V]\,\Psi = E\Psi. \tag{1}$$

Here S and V are the scalar and time-like vector potentials acting on nucleons in the nuclear medium. In the simplest version of relativistic mean field theory the scalar and vector interaction are mediated by the sigma- and omega-meson exchange, respectively. The Dirac equation has two solutions, i.e., the positive-energy solution and the negative-energy solution. For the positive-energy solution, the nucleon central potential $U_{cen} \sim V + S$ while for the negative-energy solution, due to the "G-parity" [1], the central anti-matter potential becomes $\bar{U}_{cen} \sim -V + S$. Relativistic mean-field (RMF) calculations in nuclear matter predict $V \sim 300$ MeV and $S \sim -350$ MeV [2]. In these calculations the vacuum contributions have been neglected and the definite values of V and S are parameter-dependent. If these two values for V and S are inserted into the formulae

[1]The "G-parity" is an internal symmetry of the exchanged mesons in strong interactions, which connects the NN potential $U(NN) = \sum_m V_m$ to the $N\bar{N}$ potential $U(N\bar{N}) = \sum_m G(m)V_m$. G is the combination of the isospin symmetry and the C-conjugation rule and is usually defined as $G = C\exp(-i\pi I_2)$. In particular, $G(\sigma) = G(\rho) = 1$ and $G(\omega) = G(\pi) = -1$.

of the central potentials, one immediately obtains $U_{cen} \sim -50$ MeV and $\bar{U}_{cen} \sim -650$ MeV. Therefore, the bound states of negative energy might be much deeper than the bound states of positive energy, although the exact potential depth of the bound states of negative energy has not been experimentally verified up to now. Furthermore, the vector potential V increases linearly with increasing of density. In violent relativistic heavy-ion collisions, the density may become very large, $\rho \sim 5 - 10\rho_0$. The potential of nucleons of negative energy (i.e., the anti-nucleons), may become larger than twice the nucleon's free mass with increasing density. Then, nucleons may be spontaneously emitted [3]. But nucleons will also be emitted due to the dynamics, i.e., due to the time dependent change of their orbitals, i.e., due to the Fourier frequencies of the time dependent potentials and complex scatterings in the violent compression processes of a heavy-ion collision, and also due to temperature built-up in such violent encounters. These can create a great number of nucleon holes (i.e., anti-nucleons) in bound states. Then, "clusters" of holes (anti-nucleons) are distributed over shell-model-like orbitals. They are bound by the meson fields created by the compressed matter. They are, so to speak, prepared collectively for fusion into anti-matter clusters. Again, due to the Fourier frequencies of the violent nucleus-nucleus dynamics during and after the encounter, these anti-matter clusters can be kicked into the anti-cluster continuum, i.e., the negative-energy continuum, and may escape collectively out of the reaction zone. Another possible mechanism for anti-matter cluster escaping from the reaction zone is due to the space-time dependent event by event fluctuations of N-body phase space of anti-nucleons which is not a smooth distribution function as in the case of 1-body calculations. Such collective creation processes of anti-matter clusters have a high potential to increase the probability for the production of light anti-matter clusters than the standard processes of particle scattering and coalescence.

To realize the above theoretical conjecture for the production of anti-nuclei, – and analogously also for multi-Λ, multi-$\bar{\Lambda}$ nuclei, one should answer at least three questions in a rigorous way both from the theoretical side and the experimental side: Firstly, how deep are the bound states of negative energy (i.e., the bound states of anti-nucleons) in nuclei? Secondly, how does the potential of anti-nucleons increase with the increase of density

during the violent relativistic heavy-ion collisions and what is the dynamical production procedure for the anti-matter clusters? Thirdly, can we really have stable or meta-stable (heavy) anti-nuclei? In this work, we build a model to deal with the first question, which might be extended to answer the third question as well in the future.

It is well known that relativistic mean-field theory had great success in describing the ground states of finite nuclei, i.e., the bound states of positive energy [4–7]. In this model, one usually considers only the positive-energy solution of the Dirac equation and neglects the contributions from the vacuum (the so-called *no sea approximation*). With the parameters obtained as providing the *best-fit* to the properties of spherical nuclei, such as NL1 [4] and TM1 [8] parameter sets, the model describes well the ground-state properties of spherical nuclei as well as the deformation properties of even-even nuclei. Extensive investigation of various parameter sets in connection with predicting shells for superheavy nuclei have recently been given in Ref. [9]. However, this all has been done in the no-sea approximation and without vacuum corrections. The later, the effects of quantum corrections, i.e., the vacuum contributions and their effects on the bound states of positive energy were investigated by several authors [10–14] within the local density approximation for the one-nucleon loop, the one-meson loop and for the derivative expansion for the one-nucleon loop only (in a chiral model, loop corrections have been investigated in nuclear matter e.g., in Ref. [15]). The relativistic mean-field approximation is extended to the relativistic Hartree approximation (RHA). In that version, i.e., RHA, the parameters are fitted to the saturation properties of nuclear matter as well as the rms charge radius in ^{40}Ca. The *best-fit* procedure within RHA to the properties of spherical nuclei has not been performed yet. In these preliminary studies it is found that the vacuum contributions do not improve the systematics of nuclei over RMF but the scalar density is decreased in the interior of nuclei. It, in turn, will cause the decrease of the scalar field S because the scalar field is coupled to the scalar density. Correspondingly, the vector field V will also decrease since the value $V + S$ is controlled by the saturation properties. Therefore, even if the vacuum corrections may not cause significant difference to the bound states of positive energy after refitting the parameters, they should have strong influence on the

bound states of negative energy which are sensitive to the sum of scalar and vector field $-V+S$ rather than the cancellation $V+S$ (remember: V is positive, S is negative!).

In the present paper we will develop a relativistic Hartree approach for the bound states of positive energy and negative energy in finite nuclei. The wave functions of the nucleons with positive energy are used to calculate the contributions of the valence nucleons. In principle, one should also use the wave functions of the anti-nucleons to evaluate the contributions of the bound states emerging from the Dirac sea. Considering the difficulties caused by the large number of anti-nucleons in bound states in any practical numerical procedure, we will employ the technique of derivative expansion developed in Ref. [16] to compute the effects of the Dirac sea, including the contributions of the one-nucleon loop as well as the one-meson loop. The paper is organized as follows: In Sect. II we introduce the effective Lagrangian used here. In Sect. III the plane-wave solutions of the Dirac equation in homogeneous nuclear matter are discussed. In Sect. IV we constitute the RHA approach for the bound states of positive energy and negative energy. In Sect. V we present the numerical results and discussions. Finally, a summary and outlook is given in Sect. VI.

II. EFFECTIVE LAGRANGIAN

We start from the Lagrangian density for nucleons interacting through the exchange of mesons [2,4,5]

$$\mathcal{L} = \mathcal{L}_{\rm F} + \mathcal{L}_{\rm I}. \tag{2}$$

Here $\mathcal{L}_F$ is the Lagrangian density for free nucleon, mesons and photon

$$\begin{aligned}\mathcal{L}_{\rm F} = \bar{\psi}[i\gamma_\mu\partial^\mu - M_N]\psi + \frac{1}{2}\partial_\mu\sigma\partial^\mu\sigma - U(\sigma) - \frac{1}{4}\omega_{\mu\nu}\omega^{\mu\nu} \\ + \frac{1}{2}m_\omega^2\omega_\mu\omega^\mu - \frac{1}{4}\mathbf{R}_{\mu\nu}\mathbf{R}^{\mu\nu} + \frac{1}{2}m_\rho^2\mathbf{R}_\mu\cdot\mathbf{R}^\mu - \frac{1}{4}A_{\mu\nu}A^{\mu\nu}\end{aligned} \tag{3}$$

and U(σ) is the self-interaction part of the scalar field [17]

$$U(\sigma) = \frac{1}{2}m_\sigma^2\sigma^2 + \frac{1}{3!}b\sigma^3 + \frac{1}{4!}c\sigma^4. \tag{4}$$

In the above expressions ψ is the Dirac spinor of the nucleon; σ, ω_μ, $\mathbf{R}_\mu$ and A_μ represent the scalar meson, vector meson, isovector-vector meson field and the electromagnetic field, respectively. Here the field tensors for the omega, rho and photon are given in terms of their potentials by

$$\omega_{\mu\nu} = \partial_\mu \omega_\nu - \partial_\nu \omega_\mu, \tag{5}$$

$$\mathbf{R}_{\mu\nu} = \partial_\mu \mathbf{R}_\nu - \partial_\nu \mathbf{R}_\mu, \tag{6}$$

$$A_{\mu\nu} = \partial_\mu A_\nu - \partial_\nu A_\mu. \tag{7}$$

$\mathcal{L}_I$ is the interaction Lagrangian density

$$\mathcal{L}_I = \mathrm{g}_\sigma \bar{\psi}\psi\sigma - \mathrm{g}_\omega \bar{\psi}\gamma_\mu \psi \omega^\mu - \frac{1}{2}\mathrm{g}_\rho \bar{\psi}\gamma_\mu \boldsymbol{\tau}\cdot\psi \mathbf{R}^\mu - \frac{1}{2} e\bar{\psi}(1+\tau_0)\gamma_\mu \psi A^\mu. \tag{8}$$

Here $\boldsymbol{\tau}$ is the isospin operator of the nucleon and τ_0 is its third component. g_σ, g_ω, g_ρ and $e^2/4\pi = 1/137$ are the coupling strengths for the σ-, ω-, ρ-meson and for the photon, respectively. M_N is the free nucleon mass and m_σ, m_ω, m_ρ are the masses of the σ-, ω-, and ρ-meson. For simplicity, in the following discussions we consider the σ- and ω-exchange explicitly. The relevant formulae for the ρ-exchange and the electromagnetic field can be obtained in a straightforward way after calculating the ω-exchange. The detailed expressions for all these meson fields and the electromagnetic field will be given in Sect. IV.

III. PLANE-WAVE SOLUTIONS OF THE DIRAC EQUATION IN STATIC NUCLEAR MATTER

From the effective Lagrangian given in the above section, we obtain the Dirac equation

$$\left[i\gamma_\mu \partial^\mu - \mathrm{g}_\omega \gamma_\mu \omega^\mu - M_N + \mathrm{g}_\sigma \sigma\right]\psi = 0. \tag{9}$$

In static nuclear matter, this reads

$$i\frac{\partial}{\partial t}\psi = \left[-i\boldsymbol{\alpha}\cdot\boldsymbol{\nabla} + \mathrm{g}_\omega \omega_0 + \beta(M_N - \mathrm{g}_\sigma \sigma)\right]\psi. \tag{10}$$

We know that Eq. (10) has two solutions, i.e., the positive-energy solution E_+ and the negative-energy solution E_-, which satisfy the following equations

$$(E_+ - \mathrm{g}_\omega\omega_0)\,\mathcal{U}(\mathbf{p}) = [\boldsymbol{\alpha}\cdot\mathbf{p} + \beta\,(M_N - \mathrm{g}_\sigma\sigma)]\,\mathcal{U}(\mathbf{p}), \tag{11}$$

$$(E_- - \mathrm{g}_\omega\omega_0)\,\mathcal{V}(-\mathbf{p}) = [\boldsymbol{\alpha}\cdot\mathbf{p} + \beta\,(M_N - \mathrm{g}_\sigma\sigma)]\,\mathcal{V}(-\mathbf{p}). \tag{12}$$

Here $\mathcal{U}(\mathbf{p})$ and $\mathcal{V}(\mathbf{p})$ are two spinors [18]

$$\mathcal{U}(\mathbf{p}) = N\begin{pmatrix} \chi_\sigma \\ \frac{\boldsymbol{\sigma}\cdot\mathbf{p}}{E^*(\mathbf{p})+m^*}\chi_\sigma \end{pmatrix} \qquad \mathcal{V}(\mathbf{p}) = N\begin{pmatrix} \frac{\boldsymbol{\sigma}\cdot\mathbf{p}}{E^*(\mathbf{p})+m^*}\chi_\sigma \\ \chi_\sigma \end{pmatrix}, \tag{13}$$

where N is the normalization factor and

$$m^* = M_N - \mathrm{g}_\sigma\sigma, \tag{14}$$

$$E^*(\mathbf{p}) = \sqrt{\mathbf{p}^2 + m^{*2}}. \tag{15}$$

Defining the effective positive-energy E_+^* and the effective negative-energy E_-^* as

$$E_+^* = E_+ - \mathrm{g}_\omega\omega_0 \qquad E_-^* = E_- - \mathrm{g}_\omega\omega_0, \tag{16}$$

together with Eqs. (11) $\sim$ (13) one can perform calculations similar to the free Dirac equation and obtains

$$E_+^* = E^*(\mathbf{p}) \qquad E_-^* = -E^*(\mathbf{p}). \tag{17}$$

Therefore,

$$E_+ = \sqrt{\mathbf{p}^2 + m^{*2}} + \mathrm{g}_\omega\omega_0, \tag{18}$$

$$E_- = -\sqrt{\mathbf{p}^2 + m^{*2}} + \mathrm{g}_\omega\omega_0. \tag{19}$$

The wave packet ψ can be expanded according to the plane waves of positive energy and negative energy as

$$\psi(\mathbf{x},t) = \int \frac{d^3p}{(2\pi)^{3/2}}\left(\frac{m^*}{E^*(\mathbf{p})}\right)^{1/2}\sum_{\pm s}\left[b_{\mathbf{p},s}\mathcal{U}(\mathbf{p},s)e^{i\mathbf{p}\cdot\mathbf{x}-iE_+t} + d^+_{\mathbf{p},s}\mathcal{V}(-\mathbf{p},s)e^{i\mathbf{p}\cdot\mathbf{x}-iE_-t}\right]. \tag{20}$$

The coefficient $b_{\mathbf{p},s}$ are the probability amplitudes for waves with positive energy, whereas $d^{+}_{\mathbf{p},s}$ are those for negative energy. Both the nucleons with positive energy and negative energy transport forward in time. According to the Dirac's hole theory, each particle has its partner anti-particle which transports backward in time. One can write down the corresponding equations for the anti-nucleons which have the opposite signs for the energy and momentum term compared to the eigenequations of the nucleons

$$-\left(\bar{E}_{+}+\mathrm{g}_{\omega}\omega_{0}\right)\mathcal{V}(\mathbf{p})=\left[-\boldsymbol{\alpha}\cdot\mathbf{p}+\beta\left(M_{N}-\mathrm{g}_{\sigma}\sigma\right)\right]\mathcal{V}(\mathbf{p}), \tag{21}$$

$$-\left(\bar{E}_{-}+\mathrm{g}_{\omega}\omega_{0}\right)\mathcal{U}(-\mathbf{p})=\left[-\boldsymbol{\alpha}\cdot\mathbf{p}+\beta\left(M_{N}-\mathrm{g}_{\sigma}\sigma\right)\right]\mathcal{U}(-\mathbf{p}). \tag{22}$$

Here $\bar{E}_{+}$, $\bar{E}_{-}$ are the positive energy and negative energy of the anti-nucleon and $\mathcal{V}(\mathbf{p})$, $\mathcal{U}(-\mathbf{p})$ are their corresponding eigenfunctions, respectively. Again, we define the effective positive-energy $\bar{E}^{*}_{+}$ and the effective negative-energy $\bar{E}^{*}_{-}$ of the anti-nucleon as

$$\bar{E}^{*}_{+}=\bar{E}_{+}+\mathrm{g}_{\omega}\omega_{0}\qquad\qquad\bar{E}^{*}_{-}=\bar{E}_{-}+\mathrm{g}_{\omega}\omega_{0}. \tag{23}$$

With the spinors of Eq. (13) we obtain

$$\bar{E}^{*}_{+}=E^{*}(\mathbf{p})\qquad\qquad\bar{E}^{*}_{-}=-E^{*}(\mathbf{p}) \tag{24}$$

and

$$\bar{E}_{+}=\sqrt{\mathbf{p}^{2}+m^{*2}}-\mathrm{g}_{\omega}\omega_{0}, \tag{25}$$

$$\bar{E}_{-}=-\sqrt{\mathbf{p}^{2}+m^{*2}}-\mathrm{g}_{\omega}\omega_{0}. \tag{26}$$

From Eqs. (18), (19) and (25) , (26) one can easily find the relations

$$\bar{E}_{+}=-E_{-}\qquad\qquad\bar{E}_{-}=-E_{+}. \tag{27}$$

Thus, in order to obtain the full spectrum of the Dirac equation, one can solve the equations for the nucleon with positive energy and negative energy, i.e., Eqs. (11) and (12). Alternatively, one can solve the Dirac equations for the nucleon and the anti-nucleon but both of them with positive energy, i.e., Eqs. (11) and (21). The wave packet ψ can also be expanded according to the plane waves of the nucleon and the anti-nucleon as

$$\psi(\mathbf{x},t)=\int\frac{d^3p}{(2\pi)^{3/2}}\left(\frac{m^*}{E^*(\mathbf{p})}\right)^{1/2}\sum_{\pm s}\left[b_{\mathbf{p},s}\mathcal{U}(\mathbf{p},s)e^{i\mathbf{p}\cdot\mathbf{x}-iE_+t}+d^+_{\mathbf{p},s}\mathcal{V}(\mathbf{p},s)e^{-i\mathbf{p}\cdot\mathbf{x}+i\bar{E}_+t}\right]. \quad (28)$$

Here now both the nucleon as well as the anti-nucleon have positive energy. The nucleon transports forward in time while the anti-nucleon transports backward in time which can be seen from the sign of time in exponential functions. In relativistic quantum field theory, $b^+_{\mathbf{p},s}$ and $d^+_{\mathbf{p},s}$ are explained as the creation operators for the nucleon and the anti-nucleon, respectively. This is the main strategy which will be used in our following considerations for finite nuclei. Instead of searching for two solutions with positive energy and negative energy for the Dirac equation of the nucleon, we solve the Dirac equations for the nucleon and the anti-nucleon simultaneously. For each equation we look for only one solution, that is, the positive-energy solution.

When the negative energy of the nucleon E_- is larger than the nucleon free mass, the system becomes unstable with respect to the nucleon–anti-nucleon pair creation. At zero-momentum, one has the critical condition

$$\mathrm{g}_\sigma\sigma+\mathrm{g}_\omega\omega_0=2M_N, \quad (29)$$

that is,

$$V-S=2M_N \quad (30)$$

if one defines

$$S=-\mathrm{g}_\sigma\sigma \qquad V=\mathrm{g}_\omega\omega_0. \quad (31)$$

IV. RELATIVISTIC HARTREE APPROXIMATION OF FINITE NUCLEI

In finite nuclei the meson fields in Eq. (10) are space-dependent. The field operator of the Dirac equation can be written as

$$\psi(\mathbf{x},t)=\sum_\alpha\left[b_\alpha\psi_\alpha(\mathbf{x})e^{-iE_\alpha t}+d^+_\alpha\psi^a_\alpha(\mathbf{x})e^{i\bar{E}_\alpha t}\right]. \quad (32)$$

Here the label α denotes the full set of single-particle quantum numbers. $\psi_\alpha(\mathbf{x})$ are the wave functions of nucleons and $\psi^a_\alpha(\mathbf{x})$ are those of anti-nucleons; E_α and $\bar{E}_\alpha$ are their

positive energies, respectively. b_α^+ and d_α^+ are nucleon and anti-nucleon creation operators that satisfy the standard anticommutation relations. We assume that the meson fields depend only on the radius and discuss the problem in spherically symmetric nuclei. In this case, the usual angular momentum and parity are good quantum numbers. As described in Refs. [18,19], eigenfunctions of the angular momentum and the parity operator are the well-known spherical spinors. We make the following ansatz for the wave functions of nucleons

$$\psi_\alpha(\mathbf{x}) = \begin{pmatrix} i\frac{G_\alpha(r)}{r}\Omega_{jlm}(\frac{\mathbf{r}}{r}) \\ \frac{F_\alpha(r)}{r}\frac{\boldsymbol{\sigma}\cdot\mathbf{r}}{r}\Omega_{jlm}(\frac{\mathbf{r}}{r}) \end{pmatrix} \tag{33}$$

and anti-nucleons

$$\psi_\alpha^a(\mathbf{x}) = \begin{pmatrix} \frac{\bar{F}_\alpha(r)}{r}\frac{\boldsymbol{\sigma}\cdot\mathbf{r}}{r}\Omega_{jlm}(\frac{\mathbf{r}}{r}) \\ i\frac{\bar{G}_\alpha(r)}{r}\Omega_{jlm}(\frac{\mathbf{r}}{r}) \end{pmatrix}. \tag{34}$$

Here Ω_{jlm} are the spherical spinors defined as [18]

$$\Omega_{jlm} = \sum_{m'm_s}\left(l\frac{1}{2}j \mid m'm_sm\right) Y_{lm'}\chi_{\frac{1}{2}m_s}, \tag{35}$$

$Y_{lm'}$ are the spherical harmonics and $\chi_{\frac{1}{2}m_s}$ are the eigenfunctions of the spin operators. G_α, F_α and $\bar{F}_\alpha$, $\bar{G}_\alpha$ are the remaining *real* radial wave functions of nucleons and anti-nucleons for upper and lower components, respectively. Applying the parity operator $\hat{P} = e^{i\phi}\beta\hat{P}_0$, $\hat{P}_0$ changes $\mathbf{x}$ into $-\mathbf{x}$, to Eqs. (33) and (34), one can easily find that the $\psi_\alpha(\mathbf{x})$ has the opposite eigenvalue of parity, $(-1)^l$, to the $\psi_\alpha^a(\mathbf{x})$, $(-1)^{l+1}$, as it should be [18].

Inserting Eqs. (33) and (34) into Eq. (10) ($\sigma \to \sigma(r)$ and $\omega_0 \to \omega_0(r)$), we obtain the coupled radial wave functions for the nucleon

$$E_\alpha G_\alpha(r) = \left(-\frac{d}{dr} + \frac{k_\alpha}{r}\right) F_\alpha(r) + \left(M_N - \mathrm{g}_\sigma\sigma(r) + \mathrm{g}_\omega\omega_0(r)\right) G_\alpha(r), \tag{36}$$

$$E_\alpha F_\alpha(r) = \left(\frac{d}{dr} + \frac{k_\alpha}{r}\right) G_\alpha(r) + \left(-M_N + \mathrm{g}_\sigma\sigma(r) + \mathrm{g}_\omega\omega_0(r)\right) F_\alpha(r) \tag{37}$$

and the anti-nucleon

$$-\bar{E}_\alpha \bar{F}_\alpha(r) = \left(\frac{d}{dr} + \frac{k_\alpha}{r}\right) \bar{G}_\alpha(r) + \left(M_N - \mathrm{g}_\sigma \sigma(r) + \mathrm{g}_\omega \omega_0(r)\right) \bar{F}_\alpha(r), \tag{38}$$

$$-\bar{E}_\alpha \bar{G}_\alpha(r) = \left(-\frac{d}{dr} + \frac{k_\alpha}{r}\right) \bar{F}_\alpha(r) + \left(-M_N + \mathrm{g}_\sigma \sigma(r) + \mathrm{g}_\omega \omega_0(r)\right) \bar{G}_\alpha(r) \tag{39}$$

respectively, where

$$k_\alpha = \begin{cases} -(l+1) & \text{for } j = l + \frac{1}{2} \\ l & \text{for } j = l - \frac{1}{2} \end{cases}. \tag{40}$$

In order to resemble Schrödinger equations for the Dirac equations, we eliminate the small components. For the nucleon we eliminate the lower component while for the anti-nucleon the upper component. By defining the Schrödinger equivalent effective mass and potential of the nucleon

$$M_{eff} = E_\alpha - \mathrm{g}_\omega \omega_0(r) + M_N - \mathrm{g}_\sigma \sigma(r), \tag{41}$$

$$U_{eff} = M_N - \mathrm{g}_\sigma \sigma(r) + \mathrm{g}_\omega \omega_0(r) \tag{42}$$

and the anti-nucleon

$$\bar{M}_{eff} = \bar{E}_\alpha + \mathrm{g}_\omega \omega_0(r) + M_N - \mathrm{g}_\sigma \sigma(r), \tag{43}$$

$$\bar{U}_{eff} = M_N - \mathrm{g}_\sigma \sigma(r) - \mathrm{g}_\omega \omega_0(r), \tag{44}$$

we arrive at the Schrödinger equations for the upper component of the nucleon's wave function

$$E_\alpha G_\alpha(r) = \left(-\frac{d}{dr} + \frac{k_\alpha}{r}\right) M_{eff}^{-1} \left(\frac{d}{dr} + \frac{k_\alpha}{r}\right) G_\alpha(r) + U_{eff} G_\alpha(r) \tag{45}$$

and the lower component of the anti-nucleon's wave function

$$\bar{E}_\alpha \bar{G}_\alpha(r) = \left(-\frac{d}{dr} + \frac{k_\alpha}{r}\right) \bar{M}_{eff}^{-1} \left(\frac{d}{dr} + \frac{k_\alpha}{r}\right) \bar{G}_\alpha(r) + \bar{U}_{eff} \bar{G}_\alpha(r). \tag{46}$$

The small components can be obtained through the following relations

$$F_\alpha(r) = M_{eff}^{-1} \left(\frac{d}{dr} + \frac{k_\alpha}{r}\right) G_\alpha(r), \tag{47}$$

$$\bar{F}_\alpha(r) = -\bar{M}_{eff}^{-1} \left(\frac{d}{dr} + \frac{k_\alpha}{r}\right) \bar{G}_\alpha(r). \tag{48}$$

Of course, the radial wave functions are normalized

$$\int_0^\infty dr \left[\mid G_\alpha(r) \mid^2 + \mid F_\alpha(r) \mid^2 \right] = 1, \tag{49}$$

$$\int_0^\infty dr \left[\mid \bar{G}_\alpha(r) \mid^2 + \mid \bar{F}_\alpha(r) \mid^2 \right] = 1. \tag{50}$$

From Eqs. (45) and (46) one finds that the Schrödinger equation of the anti-nucleon has the same form as that of the nucleon. The only difference relies on the definition of the effective mass and potential, that is, the vector field changes its sign. The so-called *G-parity* comes out automatically. Eqs. (45) and (46) can be solved numerically by the standard technique as described in Ref. [4]. The single-particle energy of the nucleon and the anti-nucleon can be written as

$$\begin{aligned} E_\alpha = \int_0^\infty dr \{ & G_\alpha(r) \left(-\frac{d}{dr} + \frac{k_\alpha}{r} \right) F_\alpha(r) + F_\alpha(r) \left(\frac{d}{dr} + \frac{k_\alpha}{r} \right) G_\alpha(r) \\ & + G_\alpha(r) U_{eff} G_\alpha(r) - F_\alpha(r) \left(M_{eff} - E_\alpha \right) F_\alpha(r) \}, \end{aligned} \tag{51}$$

$$\begin{aligned} \bar{E}_\alpha = \int_0^\infty dr \{ & -\bar{G}_\alpha(r) \left(-\frac{d}{dr} + \frac{k_\alpha}{r} \right) \bar{F}_\alpha(r) - \bar{F}_\alpha(r) \left(\frac{d}{dr} + \frac{k_\alpha}{r} \right) \bar{G}_\alpha(r) \\ & + \bar{G}_\alpha(r) \bar{U}_{eff} \bar{G}_\alpha(r) - \bar{F}_\alpha(r) \left(\bar{M}_{eff} - \bar{E}_\alpha \right) \bar{F}_\alpha(r) \}, \end{aligned} \tag{52}$$

which are obtained through the iteration procedure. The negative energies of nucleons are just the minus sign of $\bar{E}_\alpha$.

The meson fields in Eqs. (41) $\sim$ (44) are determined by the Laplace equations

$$\left(\boldsymbol{\nabla}^2 - m_\sigma^2 \right) \sigma(r) = -\mathrm{g}_\sigma \rho_S(r) + \frac{1}{2} b \sigma^2 + \frac{1}{3!} c \sigma^3, \tag{53}$$

$$\left(\boldsymbol{\nabla}^2 - m_\omega^2 \right) \omega_0(r) = -\mathrm{g}_\omega \rho_0(r), \tag{54}$$

where

$$\rho_S(r) = \sum_{i=-\infty}^{+\infty} w_i \bar{\psi}_i \psi_i + CT, \tag{55}$$

$$\rho_0(r) = \sum_{i=-\infty}^{+\infty} w_i \psi_i^+ \psi_i + CT, \tag{56}$$

here w_i are the occupation numbers defined by the creation and annihilation operators of Eq. (32) as usual [4]. The CT are the counterterms. The sums in Eqs. (55) and

(56) run over the full spectrum of the Dirac equation: the negative-energy continuum (the positive-energy continuum of the anti-nucleon), some negative-energy bound states (positive-energy bound states of the anti-nucleon), the positive-energy bound states which correspond to the usual nucleon shell model states and the positive-energy continuum (included through the renormalization procedure).

Let us first assume that the positive-energy continuum and the negative-energy continuum together with the contributions of the counter terms will yield finite terms for $\Delta\rho_S(r)$ and $\Delta\rho_0(r)$. The scalar and baryon density can then be expressed as

$$\begin{aligned}\rho_S(r) &= \frac{1}{4\pi r^2}\sum_\alpha w_\alpha(2j_\alpha+1)(G_\alpha^2(r)-F_\alpha^2(r)) \\ &\quad+\frac{1}{4\pi r^2}\sum_\beta w_\beta(2j_\beta+1)(\bar{G}_\beta^2(r)-\bar{F}_\beta^2(r))+\Delta\rho_S(r), \qquad (57)\\ \rho_0(r) &= \frac{1}{4\pi r^2}\sum_\alpha w_\alpha(2j_\alpha+1)(G_\alpha^2(r)+F_\alpha^2(r)) \\ &\quad-\frac{1}{4\pi r^2}\sum_\beta w_\beta(2j_\beta+1)(\bar{G}_\beta^2(r)+\bar{F}_\beta^2(r))-\Delta\rho_0(r), \qquad (58)\end{aligned}$$

The first terms on the right-hand-side of Eqs. (57) and (58) denote the contributions of the shell model states while the second terms represent the contributions of the bound states of negative energy. If one thinks about that there might exist twenty thousand nucleons in the bound states of negative energy, it is obviously not practical to compute the contributions of those bound states through evaluating their wave functions. Fortunately, a rather elegant technique has been developed by several authors [16], which takes into account the vacuum contributions to the source term of the meson fields in finite nuclei. Let us write

$$\rho_S(r) = \rho_S^{val}(r)+\rho_S^{sea}(r), \qquad (59)$$

$$\rho_0(r) = \rho_0^{val}(r)+\rho_0^{sea}(r), \qquad (60)$$

where $\rho_S^{val}(r)$ and $\rho_0^{val}(r)$ are just the first terms on the right-hand-side of Eqs. (57) and (58). $\rho_S^{sea}(r)$ and $\rho_0^{sea}(r)$ are the contributions of the vacuum, including the bound states and the continuum as well as the counterterm contributions. Originally, vacuum corrections for finite nuclei (in one-loop approximation) were included only in a local density

approximation [2]. Later on, Perry [11] and Wasson [12] considered derivative corrections to the nuclear matter results. It was found that the leading derivative correction is of the same order of magnitude as the effective potential (i.e., the nuclear matter results) while the next-order derivative correction is two or three orders of magnitude smaller than the leading order. That means that the derivative expansion converges rapidly. Since we include the non-linear self-interaction of the scalar field in the model, the contributions of the one-meson loop from the scalar meson should be taken into account in addition to the one-nucleon loop. The contributions of the one-meson loop have been calculated in Ref. [13] up to the effective potential term. Here this is extended to include the leading derivative correction.

The effective action of the system at the one-loop level can be written as

$$\Gamma = \int d^4x \left(\frac{1}{2}\partial_\mu\sigma\partial^\mu\sigma - U(\sigma) - \frac{1}{4}\omega_{\mu\nu}\omega^{\mu\nu} + \frac{1}{2}m_\omega^2\omega_\mu\omega^\mu + CT \right) + \Gamma_{\rm valence} + \Gamma^{(1)}(\sigma) + \Gamma^{(1)}(\psi). \tag{61}$$

Here $\Gamma_{\rm valence}$ is the contribution from the valence nucleons, which for time independent background fields is just minus the energy of the valence nucleons. $\Gamma^{(1)}(\sigma)$ and $\Gamma^{(1)}(\psi)$ represent the contributions of the Dirac sea stemming from the one-meson loop and one-nucleon loop, respectively. They are defined as [20]

$$\Gamma^{(1)}(\sigma) = \frac{i}{2}\hbar{\rm Tr}\ln\left[P^2 - (m_\sigma^2 + b\sigma + \frac{1}{2}c\sigma^2)\right], \tag{62}$$

$$\Gamma^{(1)}(\psi) = -i\hbar{\rm Tr}\ln\left[\not{P} - m^* - {\rm g}_\omega\not{\omega}\right], \tag{63}$$

where the trace is over spatial and internal variables. $\Gamma^{(1)}(\sigma)$ and $\Gamma^{(1)}(\psi)$ can be expanded in powers of the derivatives of the scalar and vector fields. Using Lorentz invariance one can determine the functional Taylor series as

$$\Gamma^{(1)}(\sigma) = \int d^4x \left(-V_B^{(1)}(\sigma) + \frac{1}{2}Z^{(1)}(\sigma)(\partial_\mu\sigma)^2 + Y^{(1)}(\sigma)(\partial_\mu\sigma)^4 + ... \right), \tag{64}$$

$$\Gamma^{(1)}(\psi) = \int d^4x \left(-V_F^{(1)}(\sigma) + \frac{1}{2}Z_{1\sigma}^{(1)}(\sigma)(\partial_\mu\sigma)^2 + \frac{1}{4}Z_{1\omega}^{(1)}(\sigma)\omega_{\mu\nu}\omega^{\mu\nu} + ... \right). \tag{65}$$

Here $V_B^{(1)}(\sigma)$ and $V_F^{(1)}(\sigma)$ are the effective potentials from the one-boson loop and one-fermion loop, in which the field is a constant, $\sigma(x) = \sigma_0$, the same situation as in nuclear

matter. These two terms contain divergent part and should be renormalized. Through adding the suitable counterterms, $V_B^{(1)}(\sigma)$ and $V_F^{(1)}(\sigma)$ can be evaluated in nuclear matter which turn out to be [21,2]

$$V_B^{(1)}(\sigma) = \frac{m_\sigma^4}{(8\pi)^2}\left[\left(1+\frac{b\sigma}{m_\sigma^2}+\frac{c\sigma^2}{2m_\sigma^2}\right)^2 \ln\left(1+\frac{b\sigma}{m_\sigma^2}+\frac{c\sigma^2}{2m_\sigma^2}\right) - \left(\frac{b\sigma}{m_\sigma^2}+\frac{c\sigma^2}{2m_\sigma^2}\right) - \frac{3}{2}\left(\frac{b\sigma}{m_\sigma^2}+\frac{c\sigma^2}{2m_\sigma^2}\right)^2 - \frac{1}{3}\left(\frac{b\sigma}{m_\sigma^2}\right)^2\left(\frac{b\sigma}{m_\sigma^2}+\frac{3c\sigma^2}{2m_\sigma^2}\right) + \frac{1}{12}\left(\frac{b\sigma}{m_\sigma^2}\right)^4\right], \tag{66}$$

$$V_F^{(1)}(\sigma) = -\frac{1}{4\pi^2}\left[(M_N-\mathrm{g}_\sigma\sigma)^4 \ln\left(1-\frac{\mathrm{g}_\sigma\sigma}{M_N}\right) + M_N^3\mathrm{g}_\sigma\sigma - \frac{7}{2}M_N^2\mathrm{g}_\sigma^2\sigma^2 + \frac{13}{3}M_N\mathrm{g}_\sigma^3\sigma^3 - \frac{25}{12}\mathrm{g}_\sigma^4\sigma^4\right]. \tag{67}$$

As discussed above, the derivative expansion converges rapidly. Thus, here we consider only the lowest order derivative terms in Eqs. (64) and (65). By means of the technique developed in Ref. [16], one can determine the functional coefficients of the leading derivative correction, which read

$$Z^{(1)}(\sigma) = \frac{1}{12}\frac{(b+c\sigma)^2}{16\pi^2(m_\sigma^2+b\sigma+\frac{1}{2}c\sigma^2)}, \tag{68}$$

$$Z_{1\sigma}^{(1)}(\sigma) = -\frac{\mathrm{g}_\sigma^2}{2\pi^2}\ln\left(\frac{m^*}{M_N}\right), \tag{69}$$

$$Z_{1\omega}^{(1)}(\sigma) = \frac{\mathrm{g}_\omega^2}{3\pi^2}\ln\left(\frac{m^*}{M_N}\right). \tag{70}$$

The above expressions are finite, and independent of any renormalization conditions. The divergent integral appearing in $\Gamma^{(1)}(\sigma)$ and $\Gamma^{(1)}(\psi)$ are included in the effective potential terms of $V_B^{(1)}(\sigma)$ and $V_F^{(1)}(\sigma)$. The equations of meson fields, i.e., Eqs. (53) and (54), can be obtained through minimizing the effective action of Eq. (61) with respect to the corresponding fields. With the definitions of Eqs. (57) $\sim$ (60), $\Gamma_{\rm valence}$ contributes to the $\rho_S^{val}(r)$ and $\rho_0^{val}(r)$ while $\Gamma^{(1)}(\sigma)$ and $\Gamma^{(1)}(\psi)$ contribute to the $\rho_S^{sea}(r)$ and $\rho_0^{sea}(r)$. Inserting Eqs. (64) $\sim$ (70) into Eq. (61) and minimizing the effective action, one obtains the concrete expressions of $\rho_S^{sea}(r)$ and $\rho_0^{sea}(r)$ which read

$$\rho_S^{sea}(r) = -\frac{1}{\mathrm{g}_\sigma}\frac{\partial}{\partial\sigma}\left[V_B^{(1)}(\sigma)+V_F^{(1)}(\sigma)\right] - \frac{1}{\mathrm{g}_\sigma}\left[\frac{1}{2}\frac{\partial Z^{(1)}(\sigma)}{\partial\sigma}(\boldsymbol{\nabla}\sigma)^2 - \boldsymbol{\nabla}\cdot Z^{(1)}(\sigma)\boldsymbol{\nabla}\sigma\right]$$

$$-\frac{\mathrm{g}_\sigma}{2\pi^2}\boldsymbol{\nabla}\cdot\ln\left(\frac{m^*}{M_N}\right)\boldsymbol{\nabla}\sigma-\frac{\mathrm{g}_\sigma^2}{4\pi^2 m^*}(\boldsymbol{\nabla}\sigma)^2+\frac{\mathrm{g}_\omega^2}{6\pi^2 m^*}(\boldsymbol{\nabla}\omega_0)^2, \tag{71}$$

$$\rho_0^{sea}(r)=-\frac{\mathrm{g}_\omega}{3\pi^2}\boldsymbol{\nabla}\cdot\ln\left(\frac{m^*}{M_N}\right)\boldsymbol{\nabla}\omega_0, \tag{72}$$

where

$$\begin{aligned}\frac{\partial V_B^{(1)}(\sigma)}{\partial\sigma}=&\frac{m_\sigma^4}{(8\pi)^2}\left[2\left(1+\frac{b\sigma}{m_\sigma^2}+\frac{c\sigma^2}{2m_\sigma^2}\right)\left(\frac{b}{m_\sigma^2}+\frac{c\sigma}{m_\sigma^2}\right)\ln\left(1+\frac{b\sigma}{m_\sigma^2}+\frac{c\sigma^2}{2m_\sigma^2}\right)\right.\\&\left.-2\left(\frac{b\sigma}{m_\sigma^2}+\frac{c\sigma^2}{2m_\sigma^2}\right)\left(\frac{b}{m_\sigma^2}+\frac{c\sigma}{m_\sigma^2}\right)-\frac{b^2}{m_\sigma^6}\left(b\sigma^2+2c\sigma^3\right)+\frac{b^4}{3m_\sigma^8}\sigma^3\right],\end{aligned} \tag{73}$$

$$\begin{aligned}\frac{\partial V_F^{(1)}(\sigma)}{\partial\sigma}=&-\frac{1}{4\pi^2}\left[-\mathrm{g}_\sigma\left(M_N-\mathrm{g}_\sigma\sigma\right)^3\left(1+4\ln(1-\frac{\mathrm{g}_\sigma\sigma}{M_N})\right)+M_N^3\mathrm{g}_\sigma-7M_N^2\mathrm{g}_\sigma^2\sigma\right.\\&\left.+13M_N\mathrm{g}_\sigma^3\sigma^2-\frac{25}{3}\mathrm{g}_\sigma^4\sigma^3\right]\end{aligned} \tag{74}$$

and

$$\frac{\partial Z^{(1)}(\sigma)}{\partial\sigma}=\frac{1}{192\pi^2}\left[\frac{2c(b+c\sigma)}{(m_\sigma^2+b\sigma+\frac{1}{2}c\sigma^2)}-\frac{(b+c\sigma)^3}{(m_\sigma^2+b\sigma+\frac{1}{2}c\sigma^2)^2}\right]. \tag{75}$$

Note that $\rho_0^{sea}(r)$ is a total derivative and thus the baryon number is conserved.

To include the contributions of the ρ-exchange and the electromagnetic field, in Eqs. (41) and (42) we make a replacement of

$$\mathrm{g}_\omega\omega_0(r)\longrightarrow\mathrm{g}_\omega\omega_0(r)+\frac{1}{2}\mathrm{g}_\rho\tau_{0\alpha}R_{0,0}(r)+\frac{1}{2}e(1+\tau_{0\alpha})A_0(r)$$

and in Eqs. (43) and (44)

$$\mathrm{g}_\omega\omega_0(r)\longrightarrow\mathrm{g}_\omega\omega_0(r)-\frac{1}{2}\mathrm{g}_\rho\tau_{0\alpha}R_{0,0}(r)+\frac{1}{2}e(1+\tau_{0\alpha})A_0(r).$$

Here we have defined that the anti-particle has the same isospin factor as the corresponding particle. Note that the G-parity of ρ-meson is positive. The field equations of the ρ-meson and the photon read

$$(\boldsymbol{\nabla}^2-m_\rho^2)R_{0,0}(r)=-\frac{1}{2}\mathrm{g}_\rho(\rho_{0,0}^{val}(r)+\rho_{0,0}^{sea}(r)), \tag{76}$$

$$\boldsymbol{\nabla}^2A_0(r)=-e(\rho_{Pr,0}^{val}(r)+\rho_{Pr,0}^{sea}(r)). \tag{77}$$

We assume isospin-symmetry in the bound states of negative energy, therefore, $\rho_{0,0}^{sea}(r)=0$. Other densities appearing in Eqs. (76) and (77) can be calculated with the same steps as given above. At the end we obtain

$$\rho^{val}_{0,0}(r) = \frac{1}{4\pi r^2}\sum_{\alpha} w_\alpha (2j_\alpha + 1)\tau_{0\alpha}(G^2_\alpha(r) + F^2_\alpha(r)), \tag{78}$$

$$\rho^{val}_{Pr,0}(r) = \frac{1}{2}(\rho^{val}_0(r) + \rho^{val}_{0,0}(r)), \tag{79}$$

$$\rho^{sea}_{Pr,0}(r) = -\frac{e}{6\pi^2}\boldsymbol{\nabla}\cdot \ln\left(\frac{m^*}{M_N}\right)\boldsymbol{\nabla}A_0(r). \tag{80}$$

If one includes the ρ-exchange and the electromagnetic field in Eq. (63), a term

$$\frac{e^2}{12\pi^2 m^*}(\boldsymbol{\nabla}A_0)^2$$

should be added to Eq. (71), which represents the contribution of the electromagnetic field to the derivative correction of the one-nucleon loop. The corresponding contribution of the ρ-meson field is negligible in the isospin-symmetry vacuum. The Schrödinger equations (45), (46), and the Laplace equations (53), (54), (76), (77), must be solved numerically in a self-consistent iteration procedure [4].

V. NUMERICAL RESULTS AND DISCUSSIONS

Since we employ the derivative expansion to evaluate the contributions of the Dirac sea to the source terms of the meson fields, the wave functions of anti-nucleons, which are used to calculate the single-particle energies, are not involved in evaluating the vacuum contributions to the scalar and baryon density which are, in turn, expressed by means of the scalar and vector field as well as their derivative terms. The Dirac equation of the nucleon and the equations of motion of mesons (containing the densities contributed from the vacuum) are solved within a self-consistent iteration procedure [4]. Then, the Dirac equation of the anti-nucleon is solved with the known mean fields to obtain the wave functions and the single-particle energies of anti-nucleons. The space of anti-nucleons are truncated by the specified principal and angular quantum numbers n and j with the guarantee that the calculated single-particle energies of anti-nucleons are converged when the truncated space is extended. We find that the results are insensitive to the exact values of n and j provided large enough numbers are given. We have used $n = 4$, $j = 9$ for ^{16}O; $n = 5$, $j = 11$ for ^{40}Ca; and $n = 9$, $j = 19$ for ^{208}Pb.

As pointed out in the Introduction, in the previous RHA calculations for the bound states of positive energy [10,14], the parameters of the model are fitted to the saturation properties of nuclear matter as well as the *rms* charge radius in ^{40}Ca. The *best-fit* routine within the RHA to the properties of spherical nuclei has not been performed yet. Thus, we first fit the parameters of the effective Lagrangian presented in Sect. II within the RHA to the empirical data of binding energy, surface thickness and diffraction radius of eight spherical nuclei ^{16}O, ^{40}Ca, ^{48}Ca, ^{58}Ni, ^{90}Zr, ^{116}Sn, ^{124}Sn, and ^{208}Pb as has been done in Ref. [4] for the RMF model. The experimental values for the observables used in the fit are given in Table I. In the fitting processes, we distinguish two different cases with (RHA1) and without (RHA0) nonlinear self-interaction of the scalar field. The obtained parameters and the corresponding saturation properties are given in Table II. For the sake of comparison, two sets of the linear (LIN) and nonlinear (NL1) RMF parameters from Ref. [4] are also presented. One can see that the RHA gives a larger effective nucleon mass than the RMF does, which is mainly caused by the feedback of the vacuum to the meson fields, as can be seen from Eqs. (71) $\sim$ (74). When the effective nucleon mass decreases, the scalar density originated from the Dirac sea ρ_S^{sea} increases. It is negative and cancels part of the scalar density contributed from the valence nucleons ρ_S^{val}, which causes the effective nucleon mass to increase again. At the end, it reaches a balance value. In the fitting procedure, we have tried different initial values giving smaller effective nucleon mass. After running the code many times, all of them slowly converge to a large m^*. The larger effective nucleon mass explains why a larger χ^2 value is obtained for the RHA1 compared to the NL1. If one uses the current nonlinear RMF/RHA models to fit the ground states properties of spherical nuclei, an effective nucleon mass around 0.6 is preferred. The situation, however, might be changed when other physical ingredients, e.g., tensor coupling for the vector fields, correlation effects, three-body forces, are taken into account, which warrants further investigation. On the other hand, in the case of linear model, the RHA0 gives a better fit than the LIN does. This is mainly due to the vacuum contributions which improve the theoretical results of the surface thickness substantially, and finally improve the total χ^2 value.

Fig. 1 displays the equations of state of nuclear matter as well as the scalar and vector potentials as a function of density calculated with four sets of parameters given in Table II. It is clear that the RHA exhibits a softer equation of state compared to the RMF, mainly due to the larger m^*. In the mean time, the strengths of the scalar and vector potentials decrease substantially in the RHA as expected. The same situation happens at finite nuclei. In Fig. 2 and Fig. 3 we present the scalar and vector potentials in ^{16}O, ^{40}Ca and ^{208}Pb computed with the NL1 and the RHA1 set of parameters, respectively. The potentials calculated with the RHA1 are about half of that calculated with the NL1, implying a strong feedback of the vacuum to the meson fields.

As given in Sect. IV, the contribution of the Dirac sea to the baryon density is a total derivative. The net baryon number is conserved. Fig. 4 depicts the fractions of the baryon density stemming from the vacuum in spherical nuclei of ^{16}O, ^{40}Ca and ^{208}Pb. It can be seen that the ρ_0^{sea} is more pronounced in light nuclei. In heavy nuclei it is negligible. Specifically, the $\rho_0^{sea}/\rho_0 \leq 4.0\%$ in ^{16}O, 2.3% in ^{40}Ca and 0.6% in ^{208}Pb. In Fig. 5(a) we compare the baryon densities of ^{16}O calculated within the RHA and the RMF model, respectively. One can see that the difference is not very siginificant. In the case of the RHA, the contributions of different sources to the baryon density are shown in Fig. 5(b). The vacuum contribution changes its sign from the interior to the surface of the nucleus. At large r, the Dirac-sea effect is negligible. This can be observed in Fig. 4 too. For different nuclei, after the r exceeds the typical values of surface range, the ρ_0^{sea} decreases rapidly.

In Fig. 6 the charge densities of three spherical nuclei computed with the NL1 and the RHA1 set of parameters are compared with the experimental data. It seems that for light nucleus ^{16}O the results of the NL1 are closer to the data than that of the RHA1. Alternatively, for media and heavy nuclei, the charge densities calculated with the RHA1 show a better agreement with the data and less shell fluctuation in the interior of nuclei than that with the NL1 model. The shell fluctuation can be best expressed via the charge density in ^{208}Pb as

$$\delta\rho = \rho_C(1.8 \text{ fm}) - \rho_C(0.0 \text{ fm}). \tag{81}$$

The empirical value is -0.0023 fm^{-3} [4], which is nicely reproduced in the RHA (see Table II) while the RMF overestimates $\delta\rho$ by a factor of 3, sharing the same disease with the non-relativistic mean field theory [22].

The effects of the Dirac sea on the physical quantity, specifically, the binding energy per nucleon are displayed in Table III for eight spherical nuclei. The calculations are performed with the RHA1 set of parameters. It can be found that the theoretical predictions including the vacuum contributions are in good agreement with the empirical values. The magnitudes of the Dirac-sea corrections are quite similar for different nuclei. The absolute ratios of the Dirac-sea effects and the binding energy stay between 16% and 17%. All corrections decrease the binding energy per nucleon. The contributions of the derivative terms are in the same order of magnitude as the effective potential terms. When the nucleus becomes heavier the derivative terms turn out to be smaller since the fields become more stable. In all cases, the effects of the one-nucleon-loop is about four to five times of that of the one-meson-loop.

Now let us go to the single-particle levels. In Table IV and V we present the results of both positive- and negative-energy proton and neutron spectra of ^{16}O, ^{40}Ca and ^{208}Pb. The binding energy per nucleon and the *rms* charge radius are given too. The numerical calculations are performed within two frameworks, i.e., the RHA including the contributions of the negative-energy sector to the source terms of the meson fields and the RMF taking into account only the valence nucleons as the meson-field sources. The experimental data are taken from Ref. [23]. From the table one can see that all four sets of parameters can reproduce the empirical values of the binding energies, the *rms* charge radii and the single-particle energies of positive-energy states fairly well. For the E/A and the r_{ch}, the agreement between the theoretical predictions and the experimental data are improved from the LIN to the RHA0, RHA1 and NL1 set of parameters. For the spectra of positive-energy states, due to large error bars, it seems to be difficult to queue up the different sets of parameters. However, because of the large effective nucleon mass, in the current models the RHA has smaller spin-orbit splitting (see $1p_{1/2}$ and $1p_{3/2}$ state) compared to the RMF. This situation can be improved through introducing a tensor coupling

for the ω meson [4]. With a suitable chosen coupling strength for the tensor term, a reasonable spin-orbit splitting may be obtained while a large m^* remains. The effects of the tensor-coupling terms will be investigated in the future studies. For the negative-energy sector, no experimental data are available. In all four cases, the potentials of negative-energy nucleons are much deeper than the potentials of positive-energy nucleons. On the other hand, one can notice the drastic difference between the RHA and the RMF calculations – the single-particle energies calculated from the RHA are about half of that from the RMF as can be expected from Fig. 2 and 3, exhibiting the importance of taking into account the Dirac sea effects. It demonstrates that the negative-energy spectra deserve a sensitive probe to the effective interactions in addition to the positive-energy spectra. The spin-orbit splitting of negative-energy sector is so small that one nearly can not distinguish the $1\bar{p}_{1/2}$ and the $1\bar{p}_{3/2}$ state. This is because the spin-orbit potential is related to $d(S+V)/dr$ in the negative-energy sector and two fields cancel each other to a large extent. Nevertheless, the space between the $1\bar{s}$ and the $1\bar{p}$ state is still evident, especially for lighter nuclei. This might be helpful to separate the process of knocking out a $1\bar{s}_{1/2}$ negative-energy nucleon from the background – a promising way to measure the potential of the anti-nucleon in laboratory.

Fig. 7 depicts the potentials of the anti-nucleon in ^{208}Pb computed within the NL1 and the RHA1 model. The corresponding potentials of the nucleon are presented too. One can easily find that the NL1 and the RHA1 set of parameters give the similar potentials for the nucleon (except in the center of the nucleus where the results of the RHA1 model exhibit certain fluctuations caused by the ρ_S^{sea} contributed from the vacuum) while the potentials of the anti-nucleon differ substantially. A much weaker anti-nucleon potential is obtained in the RHA1 model. This results in a large critical density (around $9.5\rho_0$) for the spontaneous nucleon–anti-nucleon pair creation as can be seen in Fig. 8 where the density dependence of the nucleon and the anti-nucleon energy in symmetric nuclear matter is given. It should be mentioned that the results of Fig. 7 and 8 are very sensitive to the effective nucleon mass which can not be determined unambiguously in a model-independent way via experiments. In order to know the individual scalar and vec-

tor potentials, one has to analyse the empirical data both from the positive-energy and the negative-energy sector. The later is, unfortunately, currently unavailable. Further investigation is apparently needed before coming to a definite conclusion.

VI. SUMMARY AND OUTLOOK

This paper develops a model to describe the bound states of positive energy and negative energy in nuclei. Instead of expanding the field operator of the Dirac equation in plane waves of nucleons with positive energy and negative energy, here the expansion is done with plane waves for nucleons and anti-nucleons separately, both of them with positive energy. In this case, the Dirac equations of both, the nucleon and the anti-nucleon, can be reduced to Schrödinger-equivalent equations. For each equation, we then search for only one solution, i.e., the positive-energy solution. The numerical procedure is similar to the one currently used in the relativistic mean field theory for the bound states of positive energy, except that one more equation for the anti-nucleon is implemented. Thus, the model is solvable with existing techniques. The single-particle energy of the nucleon with negative energy is just the negative of the single-particle energy of the anti-nucleon with positive energy, i.e., the solution of the anti-nucleon's Schrödinger equation.

The contributions of the Dirac sea to the source terms of meson fields can be separated into two parts, that is, the contributions of the negative-energy bound states and the negative-energy continuum. In principle, one should use the wave functions of anti-nucleons to evaluate the effects of the bound states emerging from the Dirac sea. There might exist a large number of anti-nucleons in bound states. Hence, it is apparently not practical to calculate all those wave functions in the iteration procedure. Here we employ the technique of derivative expansion for the one-meson and one-nucleon loop to take into account the vacuum contributions of both the bound states and the continuum.

In the numerical procedure, we first fit the parameters of the model to the properties of spherical nuclei. Two sets of parameters with and without nonlinear self-interaction of the scalar field are obtained for the present RHA model including the vacuum contributions. They are then used to investigate the vacuum polarization effects on both positive-energy

and negative-energy sector. The corresponding calculations of the RMF model are also presented for comparison. Our results show that both the RMF and the RHA model describe the properties of spherical nuclei very well. Due to the feedback of the vacuum to the meson fields, the scalar and vector potentials decrease in the RHA. This causes the drastic difference on the single-particle energies of negative-energy nucleons calculated within the RHA model and within the RMF model, while the single-particle energies of positive-energy nucleons coincide each other within two models. Since the negative-energy sector is sensitive to the sum of the scalar and vector field $-V + S$ while the positive-energy sector is sensitive to the cancellation of the fields $V + S$, the study of both of them in an unified framework will lead to the determination of the individual S and V! Thus, it is currently very important to have experimental data to check the theoretical predicted bound levels of negative energy. It will provide us with a chance to judge the physical necessity of introducing strong scalar and vector potentials in the Dirac picture. If this picture is valid for the nucleon-nucleus and anti-nucleon–nucleus interactions, a fascinating direction of future studies is to investigate the vacuum correlation and the collective production of the anti-nuclei in relativistic heavy-ion collisions. Experimental efforts in this direction are presently underway [24].

ACKNOWLEDGMENTS

The authors thank P.-G. Reinhard, Zhongzhou Ren, J. Schaffner-Bielich and C. Beckmann for stimulating discussions. G. Mao gratefully acknowledges the Alexander von Humboldt-Stiftung for financial support and the people at the Institut für Theoretische Physik der J. W. Goethe Universität for their hospitality. This work was supported by DFG-Graduiertenkolleg Theoretische und Experimentelle Schwerionenphysik, GSI, BMBF, DFG and A.v. Humboldt-Stiftung.

---

[1] W. Greiner, Heavy Ion Physics **2**, 23 (1995).

[2] B. D. Serot and J. D. Walecka, Adv. Nucl. Phys. **16**, 1 (1986).

[3] I.N. Mishustin, L.M. Satarov, J. Schaffner, H. Stöcker and W. Greiner, J. Phys. G: Nucl. Part. Phys. **19**, 1303 (1993).

[4] P.-G. Reinhard, M. Rufa, J. Maruhn, W. Greiner, J. Friedrich, Z. Phys. **A323**, 13 (1986); M. Rufa, P.-G. Reinhard, J.A. Maruhn, W. Greiner, M.R. Strayer, Phys. Rev. **C38**, 390 (1988).

[5] Y.K. Gambhir, P. Ring and A. Thimet, Ann. Phys. **198**, 132 (1990).

[6] J. Boguta, Nucl. Phys. **A372**, 386 (1981).

[7] Zhongzhou Ren, Z.Y. Zhu, Y.H. Cai, Gongou Xu, Phys. Lett. **B380**, 241 (1996).

[8] Y. Sugahara and H. Toki, Nucl. Phys. **A579**, 557 (1994).

[9] K. Rutz, M. Bender, T. Buervenich, T. Schilling, P.-G. Reinhard, J.A. Maruhn, W. Greiner, Phys. Rev. **C56**, 238 (1997); M. Bender, K. Rutz, P.-G. Reinhard, J.A. Maruhn, W. Greiner, Phys. Rev. **C58**, 2126 (1998); T.B. Buervenich, K. Rutz, M. Bender, P.-G. Reinhard, J.A. Maruhn, W. Greiner, Eur. Phys. J. **A3**, 139 (1998).

[10] C.J. Horowitz and B.D. Serot, Phys. Lett. **B140**, 181 (1984).

[11] R.J. Perry, Phys. Lett. **B182**, 269 (1986); Nucl. Phys. **A467**, 717 (1987).

[12] D.A. Wasson, Phys. Lett. **B210**, 41 (1988).

[13] W.R. Fox, Nucl. Phys. **A495**, 463 (1989).

[14] R.J. Furnstahl and C.E. Price, Phys. Rev. **C40**, 1398 (1989); Phys. Rev. **C41**, 1792 (1990).

[15] T.L. Ainsworth, G.E. Brown, M. Prakash, and W. Weise, Phys. Lett. **B200**, 413 (1988).

[16] I.J.R. Aitchison and C.M. Fraser, Phys. Lett. **B146**, 63 (1984); O. Cheyette, Phys. Rev. Lett. **55**, 2394 (1985); C.M. Fraser, Z. Phys. **C28**, 101 (1985); L.H. Chan, Phys. Rev. Lett. **54**, 1222 (1985).

[17] J. Boguta and H. Stöcker, Phys, Lett. **B120**, 289 (1983).

[18] W. Greiner, *Quantum Mechanics*, (Springer, Berlin, 1989); *Relativistic Quantum Mechanics*, (Springer, Berlin, 1990).

[19] J.D. Bjorken and S.D. Drell, *Relativistic Quantum Mechanics*, (McGraw-Hill, New York, 1964); C. Itzykson and J.-B. Zuber, *Quantum Field Theory*, (McGraw-Hill, New York, 1980).

[20] R. Jackiw, Phys. Rev. **D9**, 1686 (1974).

[21] S.A. Chin, Ann. Phys. **108**, 301 (1977).

[22] J. Friedrich and P.-G. Reinhard, Phys. Rev. **C33**, 335 (1986).

[23] J.H.E. Mattauch, W. Thiele, and A.H. Wapstra, Nucl. Phys. **67**, 1 (1965); D. Vautherin and D.M. Brink, Phys. Rev. **C5**, 626 (1972); H. de Vries, C.W. de Jager, and C. de Vries. At. Data Nucl. Data Tables **36**, 495 (1987).

[24] R. Arsenescu and the NA52 collaboration, J. Phys. **G25**, 225 (1999).

TABLE I. The experimental values for the observables included in the fit, the binding energy E_B, diffraction radius R and surface thickness σ. In the last line we also give the adopted errors ΔO_n for the fit.

	E_B (MeV)	R (fm)	σ (fm)
^{16}O	-127.6	2.777	0.839
^{40}Ca	-342.1	3.845	0.978
^{48}Ca	-416.0	3.964	0.881
^{58}Ni	-506.5	4.356	0.911
^{90}Zr	-783.9	5.040	0.957
^{116}Sn	-988.7	5.537	0.947
^{124}Sn	-1050.0	5.640	0.908
^{208}Pb	-1636.4	6.806	0.900
$\Delta O_n/O_n$	0.2%	0.5%	1.5%

TABLE II. Parameters of the RMF and the RHA models as well as the corresponding saturation properties. The results of shell fluctuation and the χ^2 values of different sets of parameters are also presented.

	RMF		RHA	
	LIN	NL1	RHA0	RHA1
M_N (MeV)	938.000	938.000	938.000	938.000
m_σ (MeV)	615.000	492.250	615.000	458.000
m_ω (MeV)	1008.00	795.359	916.502	816.508
m_ρ (MeV)	763.000	763.000	763.000	763.000
g_σ	12.3342	10.1377	9.9362	7.1031
g_ω	17.6188	13.2846	11.8188	8.8496
g_ρ	10.3782	9.9514	10.0254	10.2070
b (fm^{-1})	0.0	24.3448	0.0	24.0870
c	0.0	-217.5876	0.0	-15.9936
ρ_0 (fm^{-3})	0.1525	0.1518	0.1513	0.1524
E/A (MeV)	-17.03	-16.43	-17.39	-16.98
m^*/M_N	0.533	0.572	0.725	0.788
K (MeV)	580	212	480	294
a_4 (MeV)	46.8	43.6	40.4	40.4
$\delta\rho$ in ^{208}Pb (fm^{-3})	-0.0075	-0.0070	-0.0016	-0.0030
χ^2	1773	66	1040	812

TABLE III. Experimental and theoretical binding energy per nucleon as well as the vacuum corrections. The calculations are performed with the RHA1 set of parameters. The Dirac sea effects are separated by the effective potential terms and the derivative terms as well as the contributions of the one-nucleon-loop and the one-meson-loop.

	Exp.	Theory	Dirac Sea	Eff. Pot.	Deri. Terms	Nucl. Loop	Meson Loop
^{16}O	−7.98	−8.00	1.37	0.58	0.80	1.10	0.27
^{40}Ca	−8.55	−8.73	1.43	0.82	0.60	1.17	0.26
^{48}Ca	−8.67	−8.51	1.39	0.82	0.57	1.13	0.25
^{58}Ni	−8.73	−8.44	1.44	0.87	0.57	1.18	0.26
^{90}Zr	−8.71	−8.74	1.42	0.96	0.46	1.16	0.25
^{116}Sn	−8.52	−8.61	1.39	0.98	0.42	1.14	0.25
^{124}Sn	−8.47	−8.50	1.34	0.96	0.39	1.10	0.24
^{208}Pb	−7.87	−7.93	1.30	0.98	0.32	1.07	0.23

TABLE IV. The single-particle energies of both positive- and negative-energy protons as well as the binding energy per nucleon and the *rms* charge radius in ^{16}O, ^{40}Ca and ^{208}Pb.

	RMF		RHA		
	LIN	NL1	RHA0	RHA1	EXP.
^{16}O					
E/A (MeV)	7.80	8.00	8.01	8.00	7.98
r_{ch} (fm)	2.59	2.73	2.62	2.66	2.74
POS. ENE.					
$1s_{1/2}$ (MeV)	42.99	36.18	32.21	30.68	40±8
$1p_{3/2}$ (MeV)	20.71	17.31	16.09	15.23	18.4
$1p_{1/2}$ (MeV)	10.85	11.32	12.98	13.24	12.1
NEG. ENE.					
$1\bar{s}_{1/2}$ (MeV)	821.30	674.11	413.62	299.42	
$1\bar{p}_{3/2}$ (MeV)	754.62	604.70	369.78	258.40	
$1\bar{p}_{1/2}$ (MeV)	755.43	605.77	370.36	258.93	
^{40}Ca					
E/A (MeV)	8.38	8.58	8.65	8.73	8.55
r_{ch} (fm)	3.36	3.48	3.39	3.42	3.45
POS. ENE.					
$1s_{1/2}$ (MeV)	51.21	46.86	38.64	36.58	50±11
$1p_{3/2}$ (MeV)	35.05	30.15	27.11	25.32	
$1p_{1/2}$ (MeV)	29.25	25.11	25.17	24.03	34±6
NEG. ENE.					
$1\bar{s}_{1/2}$ (MeV)	840.76	796.09	456.58	339.83	
$1\bar{p}_{3/2}$ (MeV)	792.36	706.36	424.85	309.24	
$1\bar{p}_{1/2}$ (MeV)	792.75	707.86	425.14	309.52	
^{208}Pb					
E/A (MeV)	7.83	7.89	7.96	7.93	7.87
r_{ch} (fm)	5.34	5.52	5.43	5.49	5.50
POS. ENE.					
$1s_{1/2}$ (MeV)	58.71	50.41	44.43	40.80	
$1p_{3/2}$ (MeV)	52.74	44.45	39.87	36.45	
$1p_{1/2}$ (MeV)	51.83	43.75	39.49	36.21	
NEG. ENE.					
$1\bar{s}_{1/2}$ (MeV)	830.16	717.01	476.61	354.18	
$1\bar{p}_{3/2}$ (MeV)	819.15	705.20	466.08	344.48	
$1\bar{p}_{1/2}$ (MeV)	819.22	705.28	466.13	344.52	

TABLE V. The single-particle energies of both positive- and negative-energy neutrons.

	RMF		RHA		
	LIN	NL1	RHA0	RHA1	EXP.
^{16}O					
POS. ENE.					
$1s_{1/2}$ (MeV)	47.23	40.21	36.33	34.71	45.7
$1p_{3/2}$ (MeV)	24.70	21.07	19.99	19.04	21.8
$1p_{1/2}$ (MeV)	14.74	15.01	16.86	17.05	15.7
NEG. ENE.					
$1\bar{s}_{1/2}$ (MeV)	814.98	667.93	407.44	293.23	
$1\bar{p}_{3/2}$ (MeV)	748.48	598.74	363.83	252.48	
$1\bar{p}_{1/2}$ (MeV)	749.22	599.74	364.37	252.97	
^{40}Ca					
POS. ENE.					
$1s_{1/2}$ (MeV)	59.36	54.85	46.67	44.48	
$1p_{3/2}$ (MeV)	42.94	37.79	34.91	32.98	
$1p_{1/2}$ (MeV)	37.17	32.73	32.99	31.71	
NEG. ENE.					
$1\bar{s}_{1/2}$ (MeV)	828.82	783.87	444.85	327.96	
$1\bar{p}_{3/2}$ (MeV)	781.18	694.80	413.71	298.04	
$1\bar{p}_{1/2}$ (MeV)	781.46	696.18	413.93	298.26	
^{208}Pb					
POS. ENE.					
$1s_{1/2}$ (MeV)	65.19	58.97	50.99	47.40	
$1p_{3/2}$ (MeV)	58.50	52.44	46.05	42.66	
$1p_{1/2}$ (MeV)	57.73	51.82	45.71	42.45	
NEG. ENE.					
$1\bar{s}_{1/2}$ (MeV)	789.37	678.23	435.30	313.18	
$1\bar{p}_{3/2}$ (MeV)	779.44	667.70	425.81	304.61	
$1\bar{p}_{1/2}$ (MeV)	779.45	667.73	425.82	304.61	

FIGURE CAPTIONS

Fig.1 Equations of state of nuclear matter as well as the scalar and vector potentials calculated within the RMF and the RHA models under different sets of parameters given in Table II.

Fig.2 The scalar potentials in ^{16}O, ^{40}Ca and ^{208}Pb.

Fig.3 The vector potentials in ^{16}O, ^{40}Ca and ^{208}Pb.

Fig.4 The fractions of the baryon density contributed from the Dirac sea. The calculations are performed for ^{16}O, ^{40}Ca and ^{208}Pb with the RHA1 set of parameters.

Fig.5 The upper panel displays the baryon density in ^{16}O computed with the NL1 and the RHA1 set of parameters, respectively. The lower panel shows the contributions of the valence nucleons and the Dirac sea to the baryon density. The calculations are performed for ^{16}O with the RHA1 set of parameters.

Fig.6 The charge densities in ^{16}O, ^{40}Ca and ^{208}Pb.

Fig.7 The potentials of the nucleon and the anti-nucleon in ^{208}Pb.

Fig.8 The single-particle energies of the nucleon and the anti-nucleon as a function of density. The critical point for the NL1 is around 3.3 ρ_0 while for the RHA1 is around 9.5 ρ_0.

Fig. 1

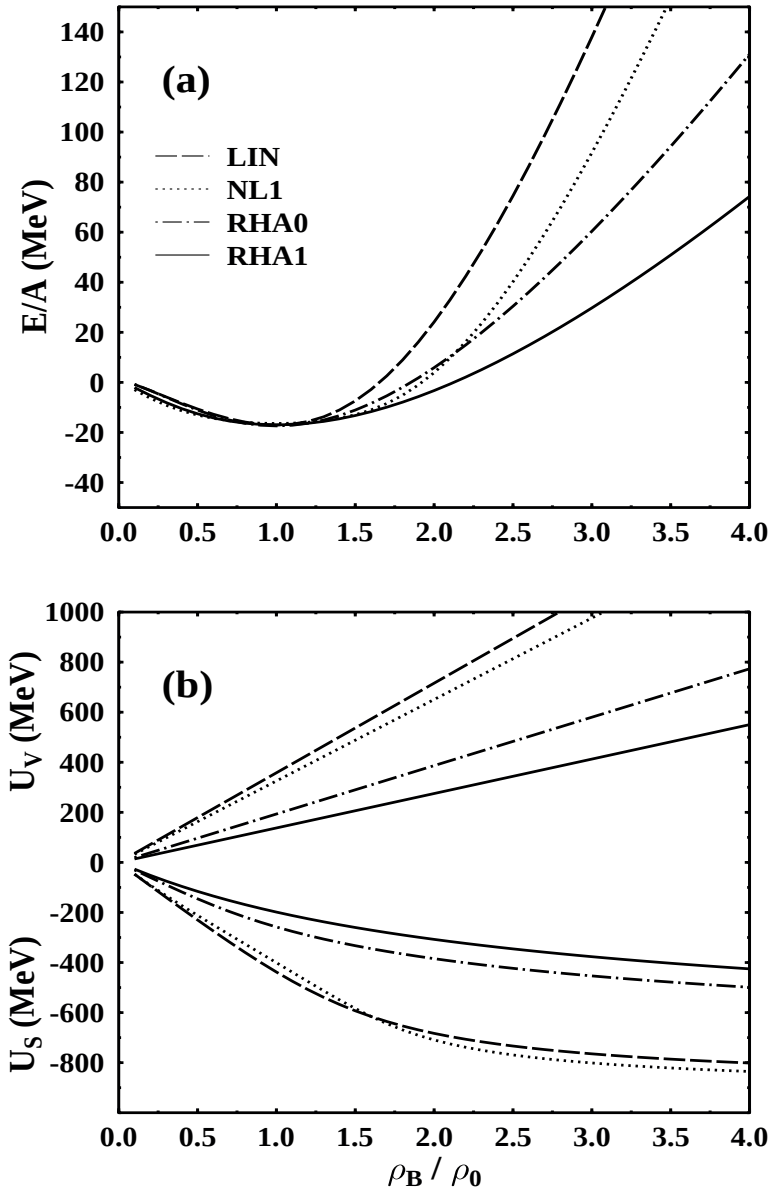
(a)
LIN
NL1
RHA0
RHA1
E/A (MeV)
140
120
100
80
60
40
20
0
-20
-40
0.0
0.5
1.0
1.5
2.0
2.5
3.0
3.5
4.0
(b)
U_V (MeV)
U_S (MeV)
1000
800
600
400
200
0
-200
-400
-600
-800
ρ_B / ρ_0

Fig. 2

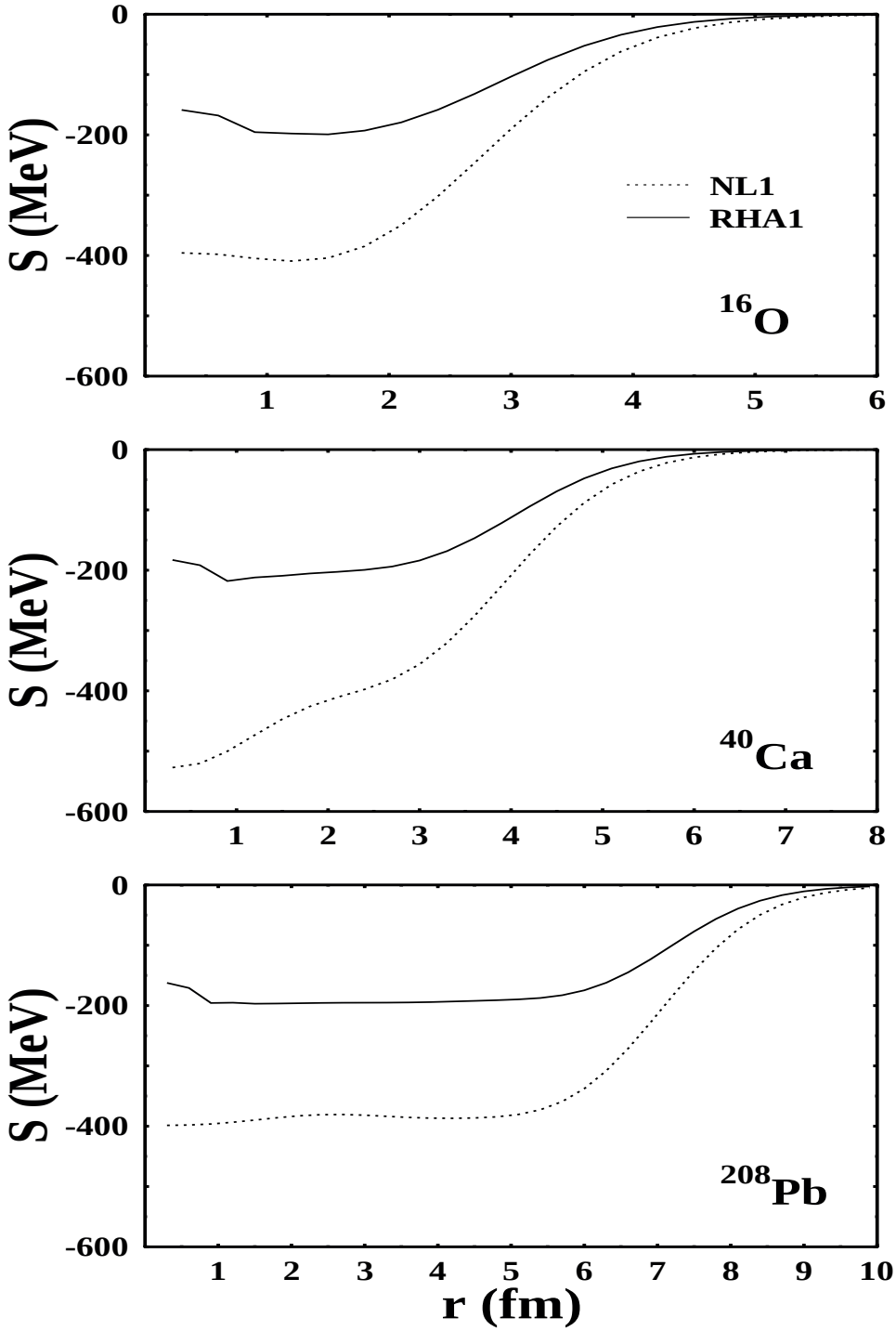
0
-200
-400
-600
S (MeV)
NL1
RHA1
^{16}O
1
2
3
4
5
6
0
-200
-400
-600
S (MeV)
^{40}Ca
1
2
3
4
5
6
7
8
0
-200
-400
-600
S (MeV)
^{208}Pb
1
2
3
4
5
6
7
8
9
10
r (fm)

Fig. 3

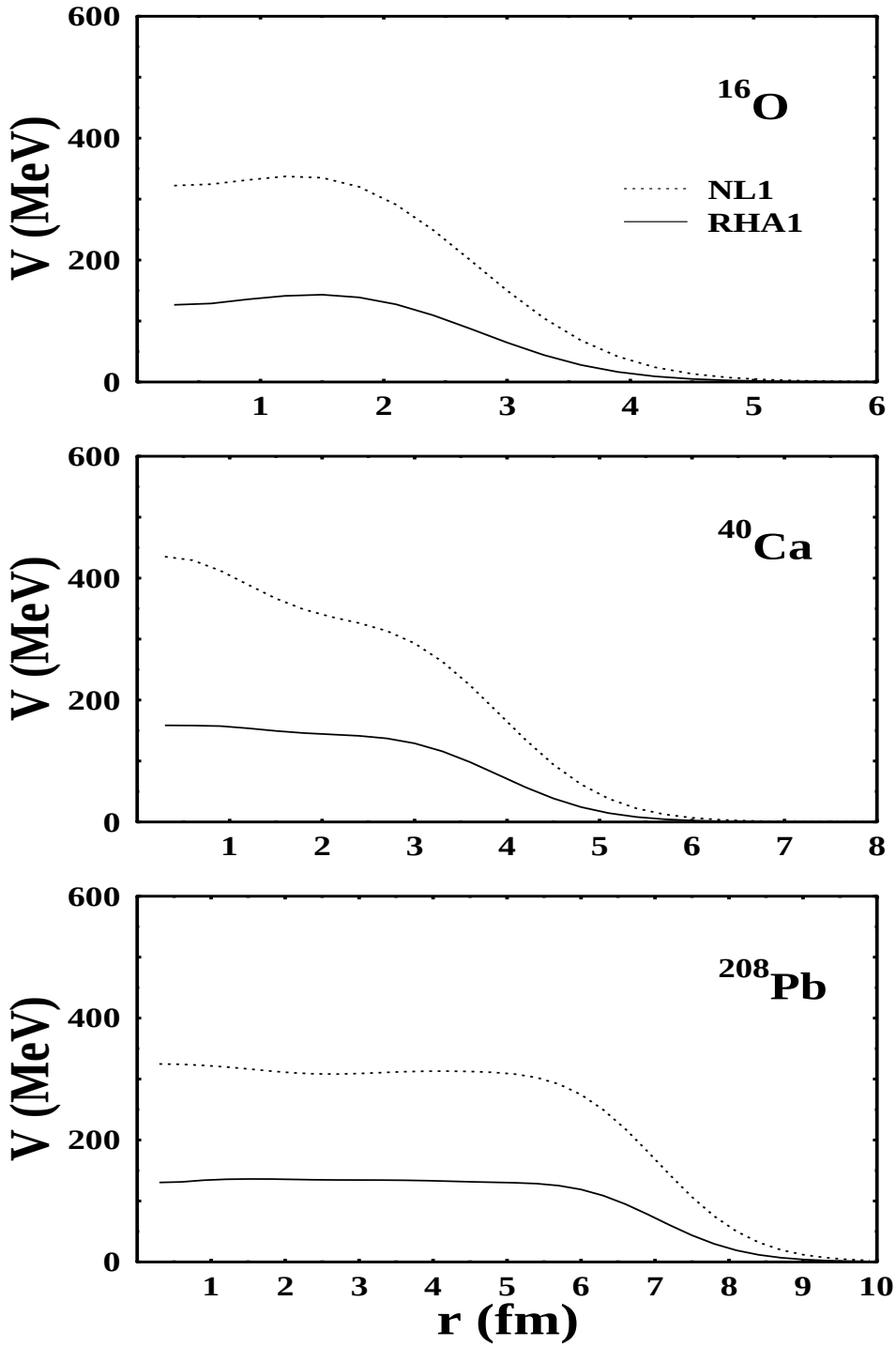
600
400
200
0
V (MeV)
^{16}O
NL1
RHA1
1
2
3
4
5
6
600
400
200
0
V (MeV)
^{40}Ca
1
2
3
4
5
6
7
8
600
400
200
0
V (MeV)
^{208}Pb
1
2
3
4
5
6
7
8
9
10
r (fm)

Fig. 4

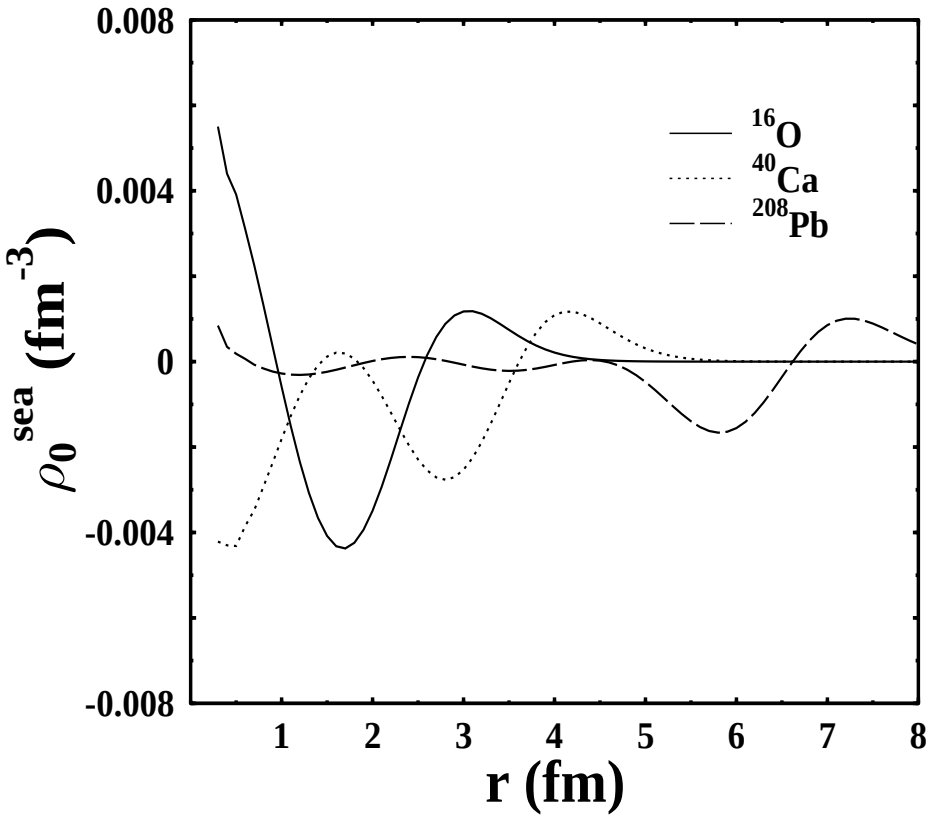
0.008
0.004
0
-0.004
-0.008
1
2
3
4
5
6
7
8
r (fm)
ρ_0^{sea} (fm^{-3})
^{16}O
^{40}Ca
^{208}Pb

Fig. 5

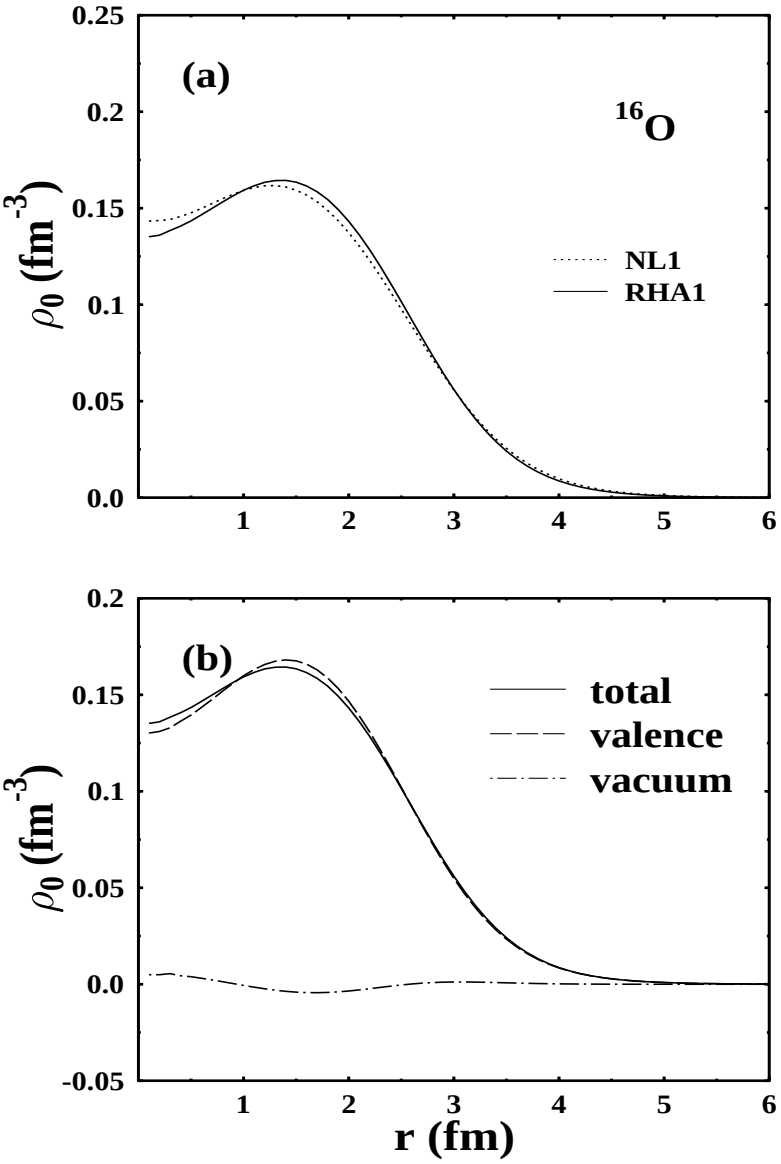

Fig. 6

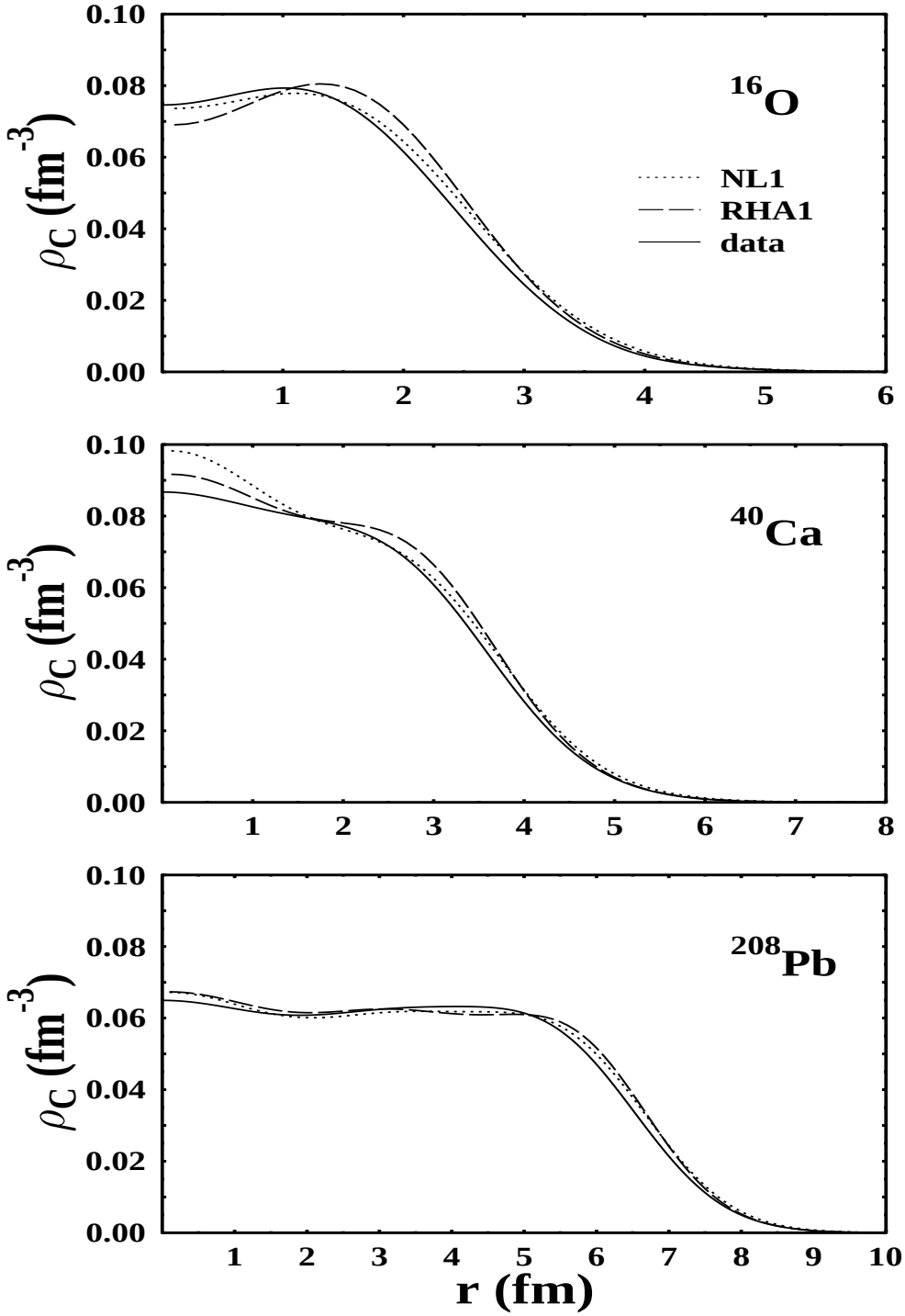
0.10
0.08
0.06
0.04
0.02
0.00
ρ_C (fm^{-3})
^{16}O
NL1
RHA1
data
1
2
3
4
5
6
^{40}Ca
7
8
^{208}Pb
9
10
r (fm)

Fig. 7

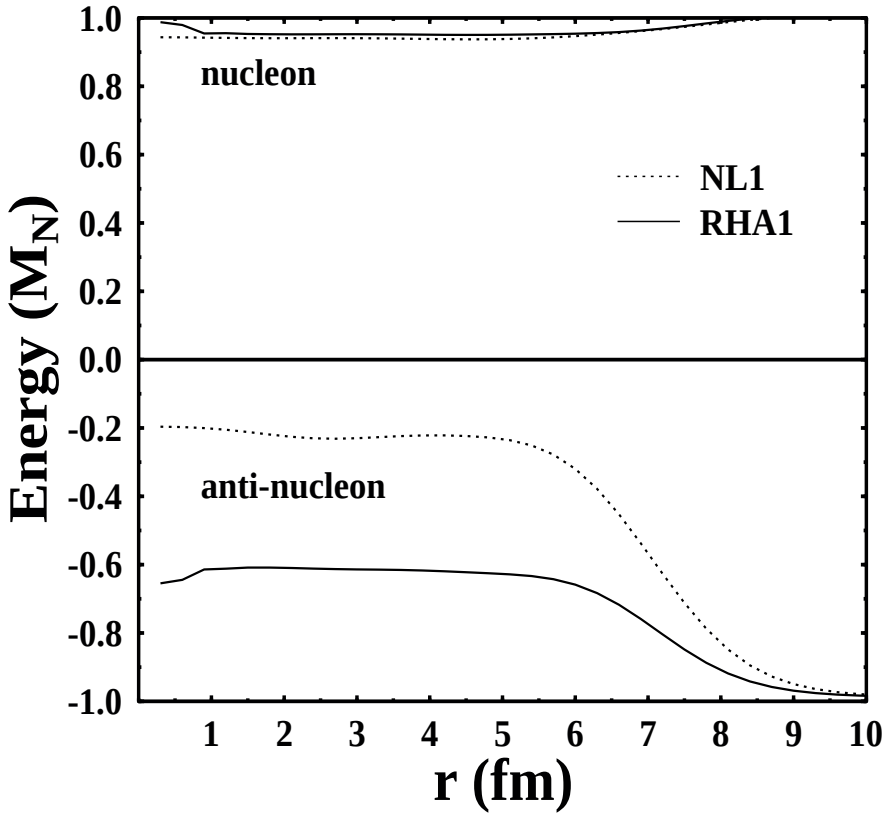
1.0
0.8
0.6
0.4
0.2
0.0
-0.2
-0.4
-0.6
-0.8
-1.0
Energy (M_N)
nucleon
anti-nucleon
NL1
RHA1
1
2
3
4
5
6
7
8
9
10
r (fm)

Fig. 8

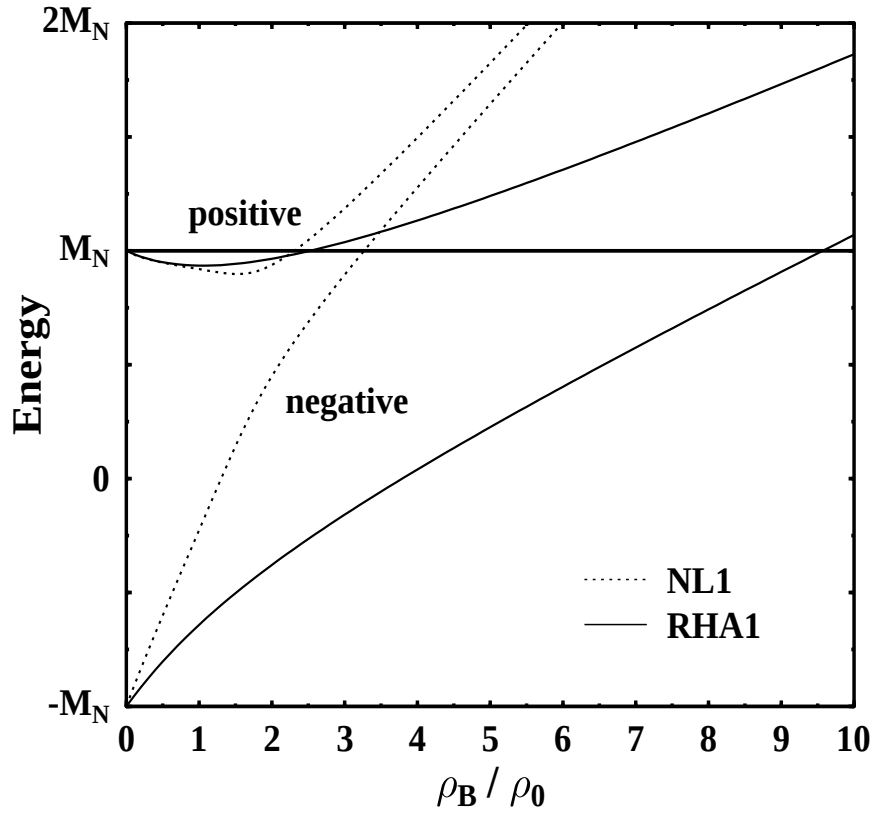
2M_N
M_N
0
-M_N
Energy
positive
negative
NL1
RHA1
0
1
2
3
4
5
6
7
8
9
10
ρ_B / ρ_0